BMC Genomics

RESEARCH Open Access

Integrated DIA proteomics and transcriptomics unravel molecular mechanisms of uterine prolificacy in Yunshang Black goats during the estrous cycle

Dongbin Zou[1], Xiaolong Du[1,2], Yufang Liu[1,3], Meiying Fang[2*] and Mingxing Chu[1*]

Abstract

Background The uterus is a pivotal organ for mammalian reproduction, directly determining reproductive success by orchestrating embryo implantation, placental development, fetal nourishment, and parturition. However, the molecular mechanisms regulating high fecundity in the uterus across different stages of the estrous cycle remain unclear. This study aimed to elucidate the genetic regulation of goat fecundity through integrated proteomic and transcriptomic analyses of uterine tissues.

Results Twenty healthy female Yunshang black goats (2–3 years old, body weight 52.22 ± 0.43 kg) were stratified into high- and low-fecundity groups during the follicular (FH and FL, $n = 5$ per group) and luteal (LH and LL, $n = 5$ per group) phases. Using data-independent acquisition (DIA) mass spectrometry, we quantified 4,455 proteins. Weighted gene co-expression network analysis (WGCNA) identified the lightcyan module as highly correlated with high fecundity in the luteal phase, with hub proteins including IDH2, PSAT1, MDH1, UBQLN1, RPLP1, SEC23B, RAD23B, PSPH, and MTHFD2. Additionally, 125 and 183 differentially abundant proteins (DAPs) were detected in the FH vs. FL and LH vs. LL comparisons, respectively. Biological adhesion processes, closely linked to transport activity, were implicated in uterine function, with key proteins such as PKP4, COL4A1, LPCAT4, ARRB1, SERPINA5, CDK9, and HDAC7 identified as potentially critical for embryo–uterine communication. Integrated transcriptomic and proteomic analyses revealed significant upregulation of the relaxin signaling pathway during the follicular phase, which may promote uterine tissue remodeling, extracellular matrix degradation, and angiogenesis, thereby facilitating preparation for embryo implantation. During the luteal phase, enhanced activity of the terpenoid backbone biosynthesis pathway was observed, which may indicate an increase in the production of cholesterol and steroid hormone precursors, potentially supporting metabolic demands and pre-receptive steroid signaling in the uterus.

Conclusion Our findings demonstrate that specific protein co-expression modules and hub proteins are closely associated with high fecundity in goats. The stage-specific activation of key pathways, including relaxin signaling and

*Correspondence:
Meiying Fang
meiying@cau.edu.cn
Mingxing Chu
mxchu@263.net

Full list of author information is available at the end of the article

terpenoid backbone biosynthesis, may reflect dynamic molecular reprogramming of the uterus during the estrous cycle. This study provides insights into the molecular mechanisms underlying uterine prolificacy in Yunshang Black goats. However, these findings are based on proteomic and transcriptomic data, and further experimental validation is needed to confirm the causal relationships.

Keywords Goat uterus, High fecundity, Estrous period, DIA proteome, Transcriptome

Introduction

The Yunshang Black goat, a novel meat breed certified by China's National Livestock Genetic Resources Committee in 2019, was developed by crossing Nubian bucks with Yunling Black does. It demonstrates exceptional reproductive performance, with adult weights reaching 76 kg (males) and 57 kg (females), and a lambing rate of 186–236%, significantly higher than that of indigenous breeds [1]. While ovarian function has been a traditional focus in fecundity research, emerging evidence suggests that the uterine microenvironment is paramount for reproductive success. In ruminants, approximately 75% of pregnancy losses are attributed to uterine dysfunction during embryo implantation [2]. The uterus plays a central role in establishing and maintaining pregnancy through cyclic endometrial remodeling, the establishment of maternal-fetal immune tolerance, and the promotion of placental formation and vascularization. These processes collectively create an essential physiological environment for embryo implantation, development, and parturition [3–5]. Nevertheless, the molecular mechanisms underlying the high fecundity of Yunshang Black goats remain poorly understood. Key questions include how the uterine microenvironment regulates maternal-fetal crosstalk through epigenetic modifications (e.g., DNA methylation), secretory factors (e.g., exosomal miRNAs), and metabolic signaling (e.g., the mTOR pathway). Elucidating these mechanisms is critical for advancing our understanding of mammalian reproductive evolution and improving goat breeding strategies [6, 7].

Recent advances in mass spectrometry (MS)-based proteomics have revolutionized the study of mammalian uterine function, enabling the deciphering of molecular processes underlying reproduction and the identification of key DAPs associated with reproductive success across species. For instance, studies in sheep have revealed critical protein interactions: the membrane protein CAPN2 is highly expressed in the endometrium, while its secretory counterpart CTSB accumulates in the conceptus. In rats, CAPN2 localizes to the basal surface of the uterine luminal epithelium during implantation, regulating focal adhesion disassembly and uterine receptivity, whereas CTSB facilitates endometrial remodeling [8]. Developmental proteomics in bovine embryos identified 140 DAPs between the morula and blastocyst stages, with upregulation of proteins such as NPM1, EIF5A, RACK1, and ANXA6, and downregulation of GSTM3, PRDX2, and AKR1B1. Notably, 73% of DAPs increased in abundance, reflecting enhanced translational activity and elevated ATP synthesis during embryonic development [9]. Similarly, proteomic analysis of uteri from Small-tailed Han sheep—grouped by litter size—identified 41 and 83 DAPs in the follicular and luteal phases, respectively. Integrated multi-omics analyses showed a positive transcriptome-proteome correlation for prolificacy traits. Functional enrichment analyses (GO/KEGG) indicated upregulation of sphingolipid and amino acid metabolism pathways in polytocous ewes compared to monotocous ewes, suggesting metabolic adaptations that support uterine function and improve embryo survival throughout the estrous cycle in highly prolific sheep [10].

Research on reproductive regulation has traditionally emphasized transcriptomic studies, which are widely employed due to their high sensitivity and cost-effectiveness. While genes act as carriers of genetic information, proteins encoded by them are the direct functional executors—highlighting the essential role of proteomics in advancing our understanding of reproductive biology. However, a growing body of evidence indicates that mRNA levels often exhibit a poor correlation with the abundance of their corresponding proteins [11]. The emergence of multi-omics technologies now empowers the assembly of expansive datasets, unlocking deeper investigation into intricate biological processes [10]. Such integrated approaches provide the resolution necessary to map the organizational principles governing mRNA and protein networks. By elucidating cellular mechanisms through complementary lenses, multi-omics holds significant potential to refine our comprehension of fundamental life processes. Conversely, a comprehensive understanding of uterine proteomic and transcriptomic dynamics across the follicular and luteal phases remains largely uncharacterized, presenting a critical knowledge gap demanding focused exploration. The Yunshang Black goat exhibits two biologically significant traits—exceptional prolificacy and year-round cyclicity—making it a valuable model for caprine reproductive physiology. In this study, we applied DIA proteomics to profile twenty uterine tissue samples, identifying key DAPs that define uterine function and genetic regulators of kidding performance. Our analyses further revealed that the estrous cycle stage is the primary factor influencing transcript and protein abundance for most uterine genes, uncovering fundamental mechanisms of mRNA-protein

concordance related to uterine reproductive efficiency in goats. Together, this integrated proteomics and transcriptomics study deciphers the molecular landscape of the uterus governing kidding capacity, identifies cycle-dependent functional networks, and highlights pivotal determinants of fertility.

Materials and methods

Animals and sample acquisition

Uterine tissue specimens were obtained from Yunshang Black goats (*Capra hircus*), a phenotypically distinct Chinese breed exhibiting exceptional fecundity, reared under standardized conditions at Yixingheng Animal Husbandry Technology Co., Ltd. (Yunnan, China). Twenty reproductively mature female goats (age: 2–5 years; body weight: 52.22 ± 0.43 kg) with significantly different prolificacy were selected based on average litter size records (at least 2 parturitions) and stratified into high-fecundity (HF: 3.3 ± 0.11 progeny per parturition, $n = 10$) and low-fecundity (LF: 1.75 ± 0.18 progeny per parturition, $n = 10$) groups.

To synchronize uterine development to a comparable stage, estrus was synchronized using intravaginal progesterone-releasing devices (CIDR inserts; 300 mg progesterone), which were maintained for 12 days. At the time of synchronization, all ewes ($n = 20$) received an intramuscular administration of 5 ml vitamin AD complex to minimize stress, maintain health status, and enhance synchronization success. Throughout the synchronization period, the ewes were group-housed under uniform management with ad libitum access to feed and water. Animals were processed in two distinct cohorts to obtain tissue samples during both the follicular and luteal phases. According to the sampling protocol, laparoscopic examinations were performed either at CIDR removal or within 48 h post-removal (targeting the follicular phase), and within 11 days post-removal (targeting the luteal phase). Ewes were euthanized promptly upon laparoscopic identification of either large, translucent follicles protruding from the ovarian surface (follicular phase cohort) or well-developed corpora lutea (luteal phase cohort). During laparoscopic examination, the number of corpora lutea was recorded and used as a phenotypic indicator to distinguish high- and low-fecundity groups, whereas follicular numbers were not quantitatively assessed in the present study. Uterine tissues were immediately collected post-mortem, rinsed with ice-cold phosphate-buffered saline (PBS), dissected free of excess adipose and connective tissue, wrapped in gauze, flash-frozen in liquid nitrogen, and subsequently stored at -80 °C for subsequent analyses.

Protein extraction and filter-aided sample preparation (FASP) for proteomic analysis

The uterine tissue was homogenized in lysis buffer using a mechanical homogenizer. The homogenate was vortex-mixed, sonicated, and incubated at 95 °C for 5 min, followed by centrifugation at 14,000×g for 40 min at 4 °C to collect the supernatant. Total protein concentration was determined using the BCA protein assay.

Protein aliquots were denatured in SDT buffer (4% SDS, 100 mM DTT, 150 mM Tris-HCl, pH 8.0) and subjected to repeated ultrafiltration with UA buffer (8 M urea, 150 mM Tris-HCl, pH 8.0) in Microcon devices to remove detergents and low-molecular-weight contaminants. Reduced cysteine residues were alkylated by adding 100 µL iodoacetamide (100 mM in UA buffer) with 30 min dark incubation. Filters were sequentially washed with UA buffer (three times) and 25 mM NH_4HCO_3 (twice). On-filter digestion was performed using 4 µg trypsin in 25 mM NH_4HCO_3 at 37 °C overnight, with resultant peptides collected and desalted on C18 columns. After vacuum centrifugation, peptides were reconstituted in 40 µL 0.1% formic acid, quantified by UV spectrophotometry at 280 nm using vertebrate-specific extinction coefficients, and fractionated into 10 fractions via Thermo Scientific™ Pierce™ High pH Reversed-Phase Peptide Fractionation Kit. All fractions were concentrated and reconstituted in 0.1% formic acid prior to spiking iRT standard peptides at a 1:3 (v/v) ratio for retention time normalization in downstream LC-MS/MS analysis.

DDA mass spectrometry assay

For DDA spectral library construction, fractionated peptides were analyzed using a Q Exactive HF-X mass spectrometer (Thermo Scientific) coupled online with an Easy nLC 1200 system. Aliquots (1.5 µg) were loaded onto a trap column (EASY-Spray™ C18, 75 µm × 2 cm, 3 µm; P/N 164946) and separated on an analytical column (EASY-Spray™ C18, 75 µm × 25 cm, 2 µm; ES802) at 250 nL/min. Separation employed a 90-min linear gradient of Buffer B (80% acetonitrile, 0.1% formic acid). Mass spectrometry operated in positive ion mode with MS1 scans (300–1800 m/z) at 60,000 resolution (200 m/z), AGC target 3e6, maximum injection time 25 ms, and dynamic exclusion 30 s. Each MS1 cycle initiated 20 ddMS2 scans at 15,000 resolution (AGC 5e4, max IT 25 ms, NCE 30 eV).

Data-independent acquisition (DIA) mass spectrometry assay

All peptide samples were subjected to LC-MS/MS analysis in DIA mode (Shanghai Applied Protein Technology). Each 90-min analytical cycle integrated one full MS-SIM scan (120,000 resolution at 200 m/z; AGC 3e6; max IT 50 ms; profile mode) with 30 variable-window DIA scans

spanning 350–1800 m/z (15,000 resolution; AGC 3e6; auto max IT; NCE 30 eV). Chromatographic separation employed a linear gradient of Buffer B (80% acetonitrile, 0.1% formic acid) at 250 nL/min. Quality control (QC) samples — generated from equal aliquots of all experimental specimens — were injected in DIA mode at initiation and post every six sample runs to monitor mass spectrometry performance stability.

Raw mass spectrometry data analysis

DDA library data were processed using MaxQuant (v1.5.3.17) against a UniProt-derived FASTA database appended with iRT peptide sequences (Biognosys|iRTKit). Search parameters specified tryptic digestion (max 2 missed cleavages), fixed carbamidomethylation (C), and dynamic modifications (oxidation (M); N-terminal acetylation). Protein identifications met 99% confidence thresholds (FDR ≤ 1% via decoy database analysis). The spectral library was constructed in Spectronaut Pulsar X (v12.0.20491.4) by integrating raw files and MaxQuant results.

DIA data analysis employed the same Spectronaut platform with these critical settings: dynamic iRT-based retention time prediction, MS2-level interference correction, and cross-run normalization. All identifications were filtered at Q < 0.01 (FDR < 1%).

Weighted gene co-expression network analysis

The WGCNA algorithm constructs weighted co-expression networks under the assumption of scale-free topology [12]. It begins by calculating a correlation matrix representing pairwise co-expression relationships among proteins. This matrix is transformed into an adjacency matrix, defining the network structure. Subsequently, a topological overlap measure (TOM) is computed to quantify network interconnectedness, mitigating spurious correlations. Hierarchical clustering based on TOM-derived dissimilarities generates a clustering tree, whose branches define distinct modules. Proteins within the same module exhibit high co-expression, while those in different modules show low co-expression. Finally, the correlation between identified protein modules and specific phenotypes or diseases is assessed to pinpoint potential therapeutically relevant targets and networks. This analysis was implemented using the WGCNA package (v1.51) in R (v3.4).

Data analysis and identification of differentially abundant proteins

We performed differential proteome analysis comparing high- versus low-fecundity goat uterus within each reproductive phase. DAPs were defined by $|\log_2(\text{fold change})| > 0.585$ (equivalent to FC > 1.5 or < 0.67) with $p < 0.05$ in paired comparisons (FH vs. FL; LH vs. LL). Volcano plots visualized significance ($-\log_{10}[p]$) against magnitude ($\pm\log_2|FC|$). Hierarchical clustering implemented in R (v3.6.3) and Java Treeview employed Euclidean distance metrics with average linkage clustering.

Functional annotation of differentially abundant proteins

Cluster analysis was performed using Cluster 3.0 (http://bonsai.hgc.jp/~mdehoon/software/cluster/software.htm) and Java Treeview (http://jtreeview.sourceforge.net) [13]. Similarity was measured using Euclidean distance, with clustering executed via the average linkage algorithm (utilizing centroid linkage). Subcellular localization of proteins was predicted using CELLO (http://cello.life.nctu.edu.tw/), a multi-class support vector machine (SVM) classification system. Protein domains within the Pfam database were identified by scanning protein sequences using InterProScan (v5.59_91.0), a tool for detecting known domains, families, and functional sites. Homologous sequences for Gene Ontology (GO) and Kyoto Encyclopedia of Genes and Genomes (KEGG) enrichment analyses were primarily obtained using NCBI BLAST, with enrichment methods consistent with those described previously [14, 15]. DAPs were defined based on a fold change threshold (|fold change| > 1.2) and statistical significance (two-tailed t-test, $P < 0.05$).

Transcriptome sequencing

High-throughput transcriptome profiling was performed on matched uterus specimens from follicular/luteal phases ($n = 20$). Total RNA was isolated using TRIzol® Reagent (Invitrogen) and subjected to stringent quality control. RNA concentration, purity ($OD_{260}/_{280}$), and spectral profiles were assessed via NanoDrop™ 2000 spectrophotometry (Thermo Fisher Scientific), with acceptance criteria requiring total RNA ≥ 3 μg, concentration ≥ 300 ng/μL, and $OD_{260}/_{280}$ ratios of 1.8–2.2. Integrity was verified through microfluidic electrophoresis (Agilent 2100 Bioanalyzer; Agilent Technologies), evaluating RIN values, 28 S/18S ratios, baseline profiles, 5 S peaks, and absence of genomic DNA contamination.

Qualified RNA specimens (RIN ≥ 8.0) underwent strand-specific cDNA library construction. Polyadenylated mRNA was enriched using oligo(dT) magnetic beads, followed by fragmentation in NEB Fragmentation Buffer with divalent cations. First-strand cDNA synthesis utilized random hexamers and M-MuLV reverse transcriptase. For strand specificity, second-strand synthesis incorporated dUTP in place of dTTP. Double-stranded cDNA underwent end repair, 3′ adenylation, and Illumina adapter ligation. Fragments of 250–300 bp were size-selected with AMPure XP beads (Beckman Coulter), followed by uracil digestion with USER enzyme (NEB) to eliminate second-strand templates prior to PCR amplification.

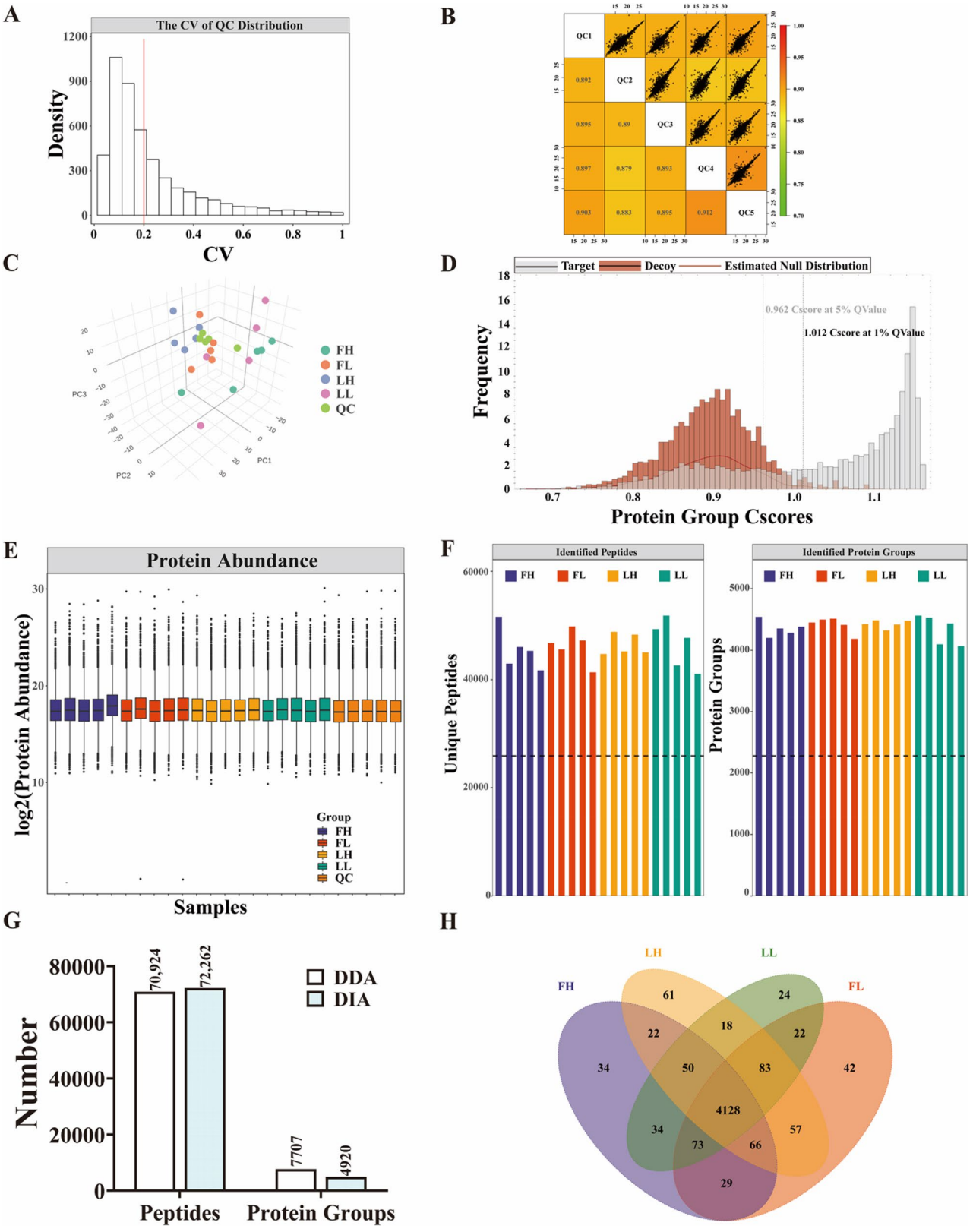

Fig. 1 (See legend on next page.)

(See figure on previous page.)

Fig. 1 Overview of quality control and quantitative proteomics. **A** Distribution of the CV across QC replicates. **B** Pearson correlation analysis among QC samples. A correlation coefficient closer to 1 indicates higher experimental stability. **C** Three-dimensional PCA of quantified proteins across all QC samples. **D** FDR analysis of protein identification. A 1% q-value threshold (equivalent to FDR ≤ 0.01) was applied. Decoy matches (anti-library) are shown in red; target matches (positive library) are in gray. The C-score reflects protein confidence, with higher values at 1% q-value indicating more reliable identifications. **E** Distribution of quantitative protein intensities across all experimental and QC samples. **F** Peptide and protein identification counts per sample. The dashed line indicates 50% of the maximum number of identifications. **G** Comparison of peptide and protein counts obtained using DDA and data-independent acquisition (DIA) strategies. **H** Venn diagram illustrating protein overlap among experimental groups

Final libraries were quantified via Qubit 2.0 Fluorometer (Thermo Fisher Scientific) and size-validated using Agilent 2100. Equimolar-pooled libraries were sequenced on the Illumina NovaSeq 6000 platform (Frasergen Bioinformatics) for 150 bp paired-end reads. Raw data underwent adapter trimming, quality filtering, and alignment to the reference genome (HISAT2 v2.1.0; parameters: --no-mixed, --no-discordant). Transcript abundance was quantified as FPKM using StringTie (v1.3.5). Differential expression analysis employed DESeq2's negative binomial model with Benjamini-Hochberg correction (significance threshold: $|\log_2 FC| \geq 0.585$, FDR-adjusted $p < 0.05$).

Correlation analyses of transcriptome and proteome profiles

We performed a multi-omics integrative analysis combining transcriptomic and proteomic data to explore regulatory mechanisms and identify potential biomarkers. DEGs from transcriptomic data were filtered using the threshold: q-value < 0.05 and FC > 2.0 (or FC < 0.5). DAPs from proteomic data were filtered according to user-uploaded criteria, with a visualization threshold of p-value < 0.05 and FC > 2.0 (or FC < 0.5). Correlation analysis was conducted on genome-wide features using expression matrices. Significantly correlated pairs were selected for further visualization. Functional interpretation of concomitant DEGs and DAPs was supported by Gene Ontology (GO) and KEGG pathway enrichment analyses, alongside GSEA to reveal coordinated regulation at both transcriptional and translational levels.

Statistical analysis

Prior to statistical analyses, data distribution normality was assessed using Shapiro-Wilk testing. Based on these results, differential expression in FH vs. FL and LH vs. LL cohorts was evaluated by Student's t-test. All computations were performed in IBM SPSS Statistics (v25.0) with data visualization implemented in GraphPad Prism (v9.3.1). Spearman rank correlation analysis examined transcriptome-proteome relationships in uterus tissues. Experiments employed ≥ 3 biological replicates, with data presented as mean ± SEM. Significance thresholds followed standard conventions: $^{*}P < 0.05$, $^{**}P < 0.01$, $^{***}P < 0.001$.

Results

Overview of quantitative proteomics analysis of goat uterus

Proteome sequencing showed that the median intra-group coefficient of variation (CV) for the four quality control (QC) replicates was approximately 20% (Fig. 1A). Pearson correlation analysis at the protein level indicated high reproducibility among the five QC replicates, with a correlation coefficient of approximately 0.9 (Fig. 1B). Principal component analysis (PCA) demonstrated clear separation among the four experimental groups and QC samples, with good clustering of samples within the same stage (Fig. 1C). DIA-based quality control results are provided in Supplementary Figure S1. The false discovery rate (FDR) method was used for multiple testing correction, with a *q*-value threshold of 0.01 (equivalent to FDR < 0.01). The C-score was 1.012 with a q-value < 0.01, indicating high confidence in protein identification (Fig. 1D). Furthermore, protein expression abundance was consistent across the five biological replicates within each group (Fig. 1E), confirming the high reproducibility of the DIA-MS data.

In this study, each sample was quantified, and we selected proteins at constant levels found in more than 50% of samples for follow-up statistics (Fig. 1F, Supplementary Data1). In total, 70,924 peptides and 7,707 proteins were quantified in the data-dependent acquisition (DDA) spectral library (Fig. 1G). Subsequent analysis of DIA data using the DDA library via Spectronaut Pulsar X led to the quantification of approximately 72,262 peptides and 4,920 proteins (Fig. 1G, Supplementary Data1). A heatmap of all DIA-identified proteins is shown in Supplementary Figure S1D. Among these, 4,128 proteins were common to all four groups (Fig. 1H).

Uterus protein co-expression network analysis identifies module-trait relationships and hub proteins of fecundity

In total, 4455 proteins were screened from the 4920 to reveal the expression patterns of proteins inside various WGCNA modules following the determination of a soft threshold at $R^2 = 0.9$ (Supplementary Data S2). Subsequently, average linkage hierarchical clustering identified 34 modules across the four groups, as visualized in Fig. 2A (Supplementary Data S2). The co-expression heatmap further demonstrated that proteins within the same module exhibit strong biological coherence (Fig. S2A, Supplementary Data S2). To assess the significance

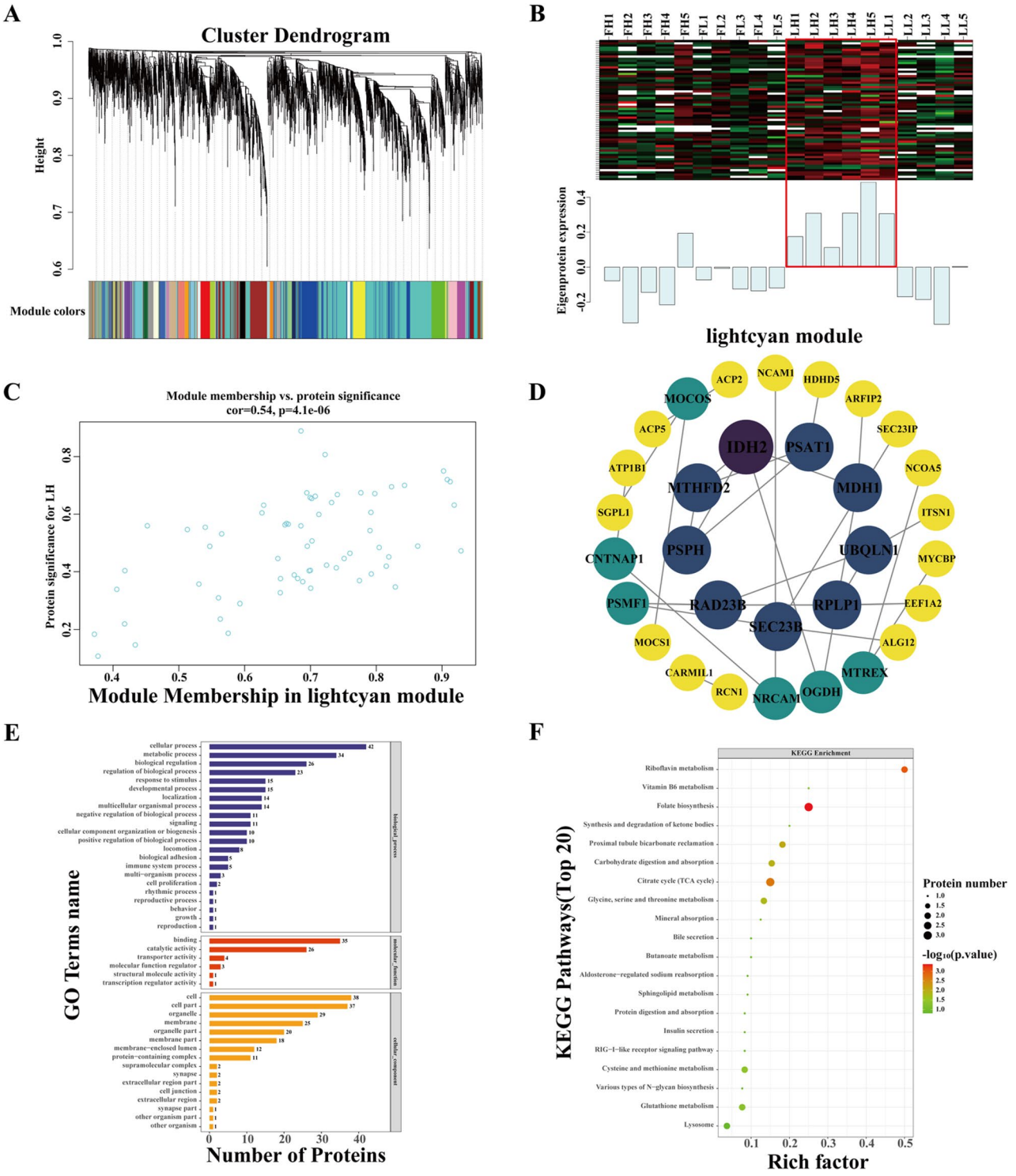

Fig. 2 Protein co-expression network analysis of the uterus proteome identified modules associated with high fecundity. **A** Module colors represent the final modules. Each branch in the hierarchical tree or each vertical line in the color bars represents one protein. **B** Eigengene expression pattern of the lightcyan module. **C** A scatterplot of proteins significance for high fecundity in the luteal phase (LH) vs. module membership in the lightcyan module. **D** The co-expressed protein network of the lightcyan module. **E** GO analysis of lightcyan module proteins. The vertical coordinate indicates the GO Level 2 annotation information, including Biological Process, Molecular Function, and Cellular Component; the horizontal coordinate indicates the number of DAPs under each functional category. **F** KEGG enrichment analysis of lightcyan module proteins

of the modules with prolificacy traits, we correlated the modules with fecundity hall-marks of goats in the different estrus cycles (Fig. S2B, Supplementary Data S2). In the follicular phase, the darkgreen module (52 proteins, cor = – 0.64, and $p = 0.002$) negatively correlated with the trait of high fecundity (FH); midnightblue modules (70 proteins, respectively; cor = 0.55, and $p = 0.01$) showed the highest correlation with low fecundity (FL). In the luteal phase, the lightcyan module (64 proteins, cor = 0.72, and $p < 0.001$) and steel-blue module (38 proteins, cor = 0.53, and $p = 0.02$) showed the strongest correlation with the trait of high (LH) and low (LL) fecundity, respectively. These modules suggest that the proteins in the modules were significantly associated with the corresponding trait. Of note, the lightcyan module had a significantly positive correlation with the high-fecundity trait in the luteal phase and was selected for further analysis ($p < 0.05$) (Fig. 2B, Supplementary Fig. S2B). The scatter plot demonstrated that the significance and module membership of the correlated proteins in the lightcyan modules were significantly associated with LH, as shown in Fig. 2C. We built a protein-protein interaction (PPI) network using Cytoscape software (V.3.9.0) for the lightcyan module with several hub proteins with the most connectivity (Fig. 2D, Supplementary Data S2). Several top hub proteins in this module play indispensable roles in cellular metabolism, epigenetic regulation, protein synthesis and trafficking, and maintenance of DNA repair protein homeostasis, including IDH2, PSAT1, MDH1, UBQLN1, RPLP1, SEC23B, RAD23B, PSPH, and MTHFD2.

In addition, the gene ontology (GO) databases were used to analyze the functional of lightcyan module proteins based on three categories, including biological process (GO BP), cellular component (GO CC), and molecular function (GO MF) (Fig. 2E, Supplementary Data S3). In the GO BP category, the most prevalent functions were cellular processes, metabolic processes, and biological regulation. Growth and reproduction were less prominent. In the GO MF category, binding and catalytic activity were the most abundant groups. The GO CC categories were dominated by proteins associated with cell, cell parts, organelle, and membrane. SGPL1, SLC37A4, TMEM65, CNTNAP1, MGP, ANXA3, ACP5, NDRG4, CARMIL1 were enriched in the reproductive process, reproduction, biological regulation, and development process, which may be significantly associated with the fecundity of the goat. In the KEGG enrichment analysis, the Folate biosynthesis pathway was the most significantly enriched (Fig. 2F, Supplementary Data S3), and MOCOS, MOCS1 and PCBD1 participated in this pathway.

Identification of differentially abundant proteins

A total of 4296 and 4279 proteins were identified in the FH vs. FL and LH vs. LL comparisons, respectively, while 125 and 183 DAPs were identified in each comparison group. In the FH vs. FL comparison group, 77 of these DAPs showed upregulation, 48 showed downregulation (Fig. 3A, Supplementary Data S1), and 99 showed upregulation; 84 showed down-regulation in the LH vs. LL comparison group (Fig. 3B). DAPs were further selected to build a heatmap (Fig. 3C, D), which revealed the expression patterns in the follicular and luteal phases of goat uterus. Moreover, the similarity of data patterns within each group is high, while it is low between groups, which effectively differentiates the groups. Protein expression changes categorized by fold-change (FC). Follicular phase (FH vs. FL): 76 upregulated (FC 1.5–10), 1 extremely upregulated (FC > 10), 47 downregulated (FC 0.1–0.667). Luteal phase (LH vs. LL): 93 upregulated, 6 extremely upregulated, 80 downregulated, 4 extremely downregulated (FC < 0.1) (Fig. 4A). These results suggested that the follicular phase of the uterus and luteal phase have different protein profiles in response to the prolificacy trait of goats.

Bioinformatic analysis of DAPs

The subcellular localization, domain enrichment, GO annotation, and Kyoto encyclopedia of genes and genomes (KEGG) enrichment analysis were used to understand the functions of the DAPs. We performed subcellular fractionation analyses, which revealed that 125 and 183 DAPs were classified into six subcellular localization categories in the FH vs. FL and LH vs. LL groups, respectively. In the FH vs. FL comparison groups, a total of 57 DAPs were localized to the nuclear (45.6%), followed by the cytoplasmic (41.6%). Regarding the LH vs. LL comparison, the subcellular localizations were like those in the FH vs. FL comparison of DAPs (Fig. 4B, C). Domain enrichment revealed that DAPs between FH and FL mainly included the Acyltransferase, Guanylate kinase, and some other domains ($p < 0.01$) Meanwhile, the most enriched domains in the LH vs. LL were the C2 domain, Ubiquitin family ($p < 0.01$), etc. (Fig. 4D, E). GO enrichment analysis of all DAPs revealed that they were mostly localized in the cell part, and a large number of DAPs were mainly involved in molecular function with binding ability, catalytic activity, and molecular function regulator (Supplementary Data S3). Among the annotated terms of the FH vs. FL comparison group (Fig. 5A), in the group within the GO BP category, a few DAPs were localized to biological adhesion, behavior, locomotion, and cell aggregation, while many DAPs were assigned to respond to the negative regulation of biological processes.

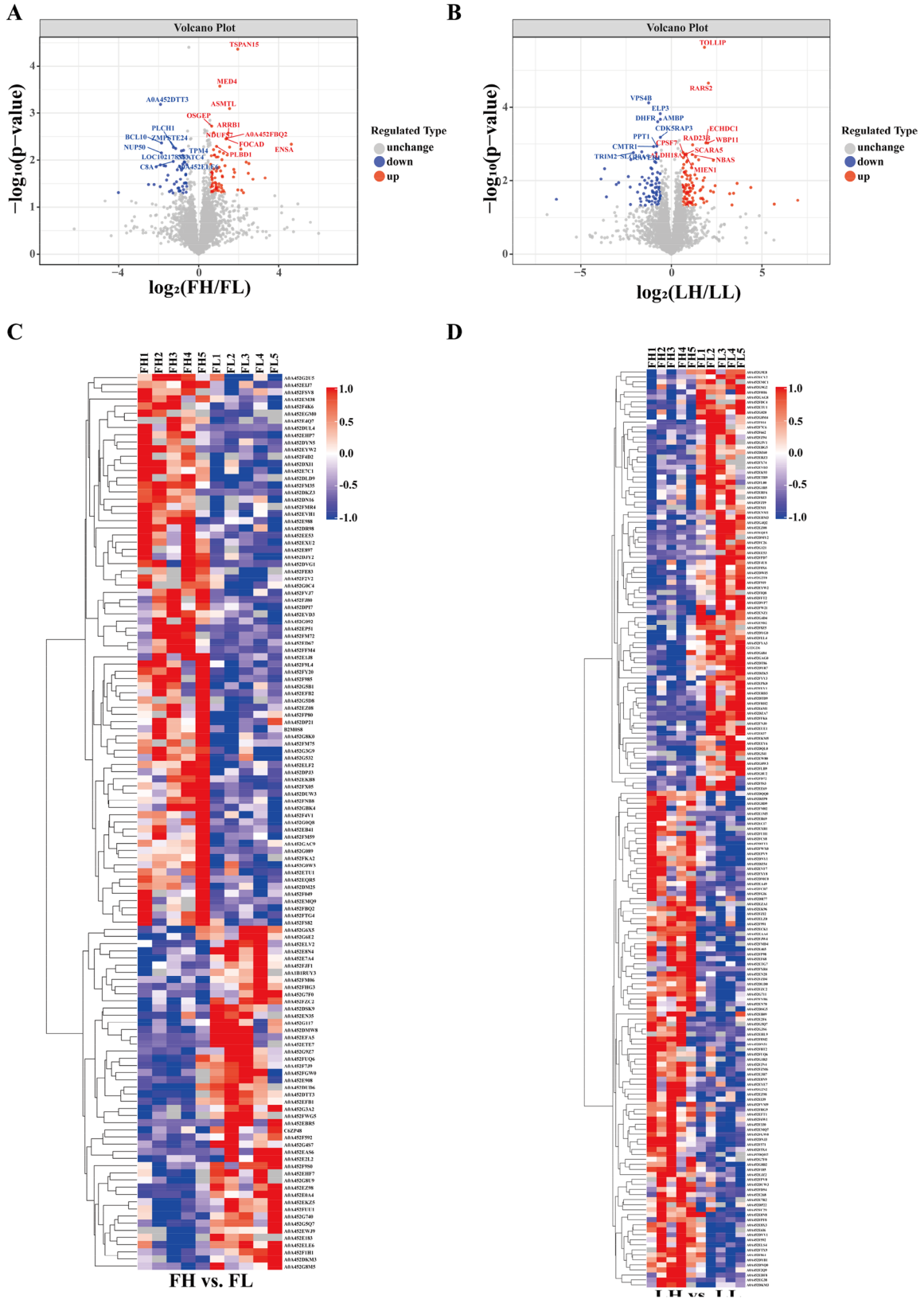

Fig. 3 (See legend on next page.)

(See figure on previous page.)

Fig. 3 Screening and cluster analysis of DAPs. **A**, **B** Volcano plot of DAPs in the two comparison groups of FH vs. FL (**A**) and LH vs. LL (**B**). The X-axis represents the fold change in protein expression of different comparison groups. The Y axis represents the statistical significance of proteins. The blue dots represent the proteins that were not significantly downregulated, the red dots represent proteins that were significantly upregulated, and the gray dots represent proteins that were not significantly different. **C**, **D** Hierarchical clustering heatmaps of DAPs in FH vs. FL (**C**) and LH vs. LL (**D**). Rows correspond to DAPs, and columns represent samples. Red indicates upregulation, blue indicates downregulation, and gray represents missing quantitative values

At the GO CC category level, 16 major processes were discovered from the DAPs, including the cell part, cell, and organelle. Binding, catalytic activity, and molecular function regulators were predominant in GO MF. Meanwhile, the main enriched GO categories in the case of LH vs. LL (Fig. 5B) were essentially the same as in the FH vs. FL comparison groups. Noticeably, transmembrane protein 119 (TMEM119) was enriched in the BP category of the reproductive process (GO:0022414), reproduction (GO:0000003), developmental process (GO:0032502) and cell proliferation (GO:0008283) similar to the LH vs. LL comparison groups. As for the KEGG pathway analysis in the FH vs. FL, DAPs were enriched in ribosome biogenesis in eukaryotes, endocytosis, wnt signaling pathway, and thermogenesis ($p < 0.01$) (Fig. 5C, Supplementary Data S3). In terms of LH vs. LL comparison, the pathways with the highest number of DAPs were the endocytosis, lysosome, and RNA transport (Fig. 5D, Supplementary Data S3). As noted above, the GO categories and KEGG pathways provided further clues to the molecular mechanisms of the uterus underlying goat prolificacy.

PPI network analysis for goat prolificacy trait

In the FH vs. FL comparison, an interaction network was constructed (Fig. 6A, Supplementary Data S3), where proteins centrally located (hubs) exhibited stronger connectivity than those at the periphery. Significantly enriched interactions were observed among 47 DAPs, with SIL1, APMAP, INTS11, IFI35, DNAJC10, NAPG, CGNL1, PUDP, MRE11, EFL1, and ASMTL identified as hub proteins within this network. Meanwhile, the LH vs. LL comparison revealed an interaction network comprising 90 DAPs. Hub proteins central to the distinct clusters of this network included ALDH18A1, POLR1B, BYSL, SYMPK, ITSN1, TSR1, NAT10, HTT, CSTF3, and PSPH (Fig. 6B, Supplementary Data S3). Furthermore, box plots illustrating the expression levels of key differentially abundant proteins (Fig. 6C-F).

Combined analysis of proteome and transcriptome (DAPs/DEGs) responding to prolificacy trait of Yunshang Black goat in uterus

Comparing the two phases, our transcriptomics and proteomics results showed that many more transcripts could be identified than proteins in the uterus. In total, 61,446 and 62,158 genes were detected from an RNA-seq analysis in goat uterus in the follicular and luteal phases after stringent quality checks and data analysis, respectively, whereas the number of detected proteins was 4240 and 4226. An integrated analysis of proteomic and transcriptomic pro-filing screened 3,703 and 3,695 genes overlapping in the mRNA and protein levels in the two phases, respectively (Fig. 7A, B, Supplementary Data S4). Comparing the FH group with the FL group revealed 1758 differentially expressed genes (DEGs; 949 upregulated/809 downregulated), and 125 DAPs (77 upregulated/48 downregulated) were identified. In LH vs. LL comparison groups, 3072 DEGs (1172 upregulated/1900 downregulated) and 183 DAPs (99 upregulated/84 downregulated) were identified (Fig. 7A, B).

In the FH vs. FL comparison, GSEA of proteomic and transcriptomic data revealed significant enrichment in pathways such as the relaxin signaling pathway and terpenoid backbone biosynthesis (Fig. 7C, Supplementary Data S4). Notably, the relaxin signaling pathway showed opposing enrichment directions between the two omics layers, while the terpenoid backbone biosynthesis pathway exhibited consistent enrichment but with markedly different magnitudes (Fig. 7D, Supplementary Data S4). These results suggest potential post-transcriptional regulatory mechanisms underlying the observed discordance. In the LH vs. LL comparison, GSEA identified significant enrichment in pathways including but not limited to steroid hormone biosynthesis and hedgehog signaling pathway (Fig. 7E, Supplementary Data S4). Further analysis revealed that the hedgehog signaling pathway showed discordant enrichment between transcriptomic and proteomic profiles, while the steroid hormone biosynthesis pathway was consistently enriched but to differing degrees (Fig. 7F, Supplementary Data S4). Additional pathways including riboflavin metabolism, proteasome, and complement and coagulation cascades were also significantly enriched.

Discussion

Mammalian reproduction is a highly complex process that depends on precise molecular coordination across multiple reproductive organs. This study employed a DIA-based proteomic approach integrated with bioinformatics to investigate key molecular mechanisms underlying the high fecundity of Yunshang Black goat uteri during the estrous cycle. We established a comprehensive proteomic profile of the goat uterus and identified DAPs across different stages of the estrous cycle. These DAPs are closely associated with critical physiological functions, including cell adhesion processes essential

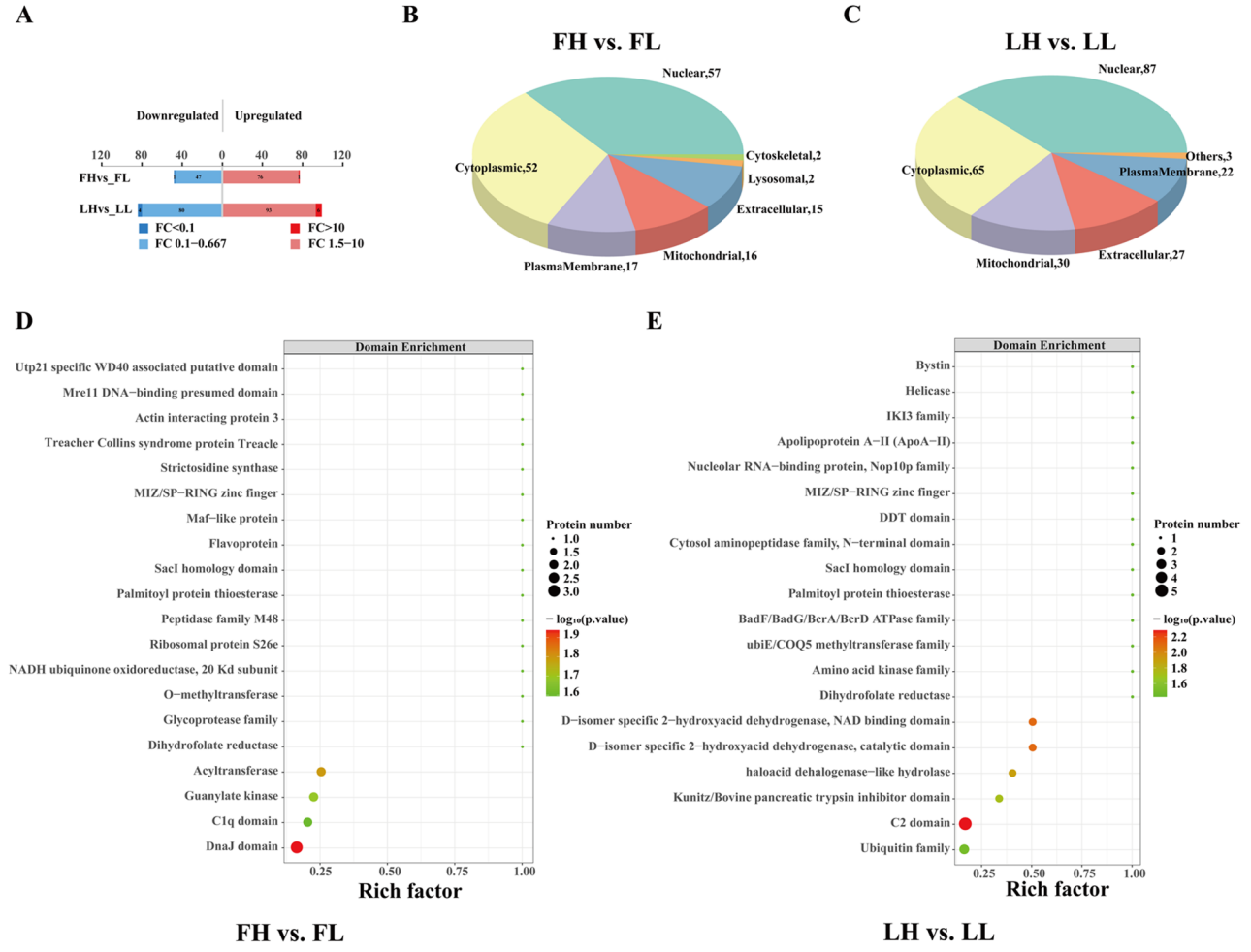

Fig. 4 Functional annotation analysis of DAPs. **A** Statistical summary of DAPs identified in the uterine tissues during follicular and luteal phases. **B** Subcellular localization of DAPs in uterine tissue during the follicular phase. **C** Subcellular localization of DAPs in uterine tissue during the luteal phase. **D**, **E** Domain enrichment analysis of DAPs in the FH vs. FL (**D**) and LH vs. LL (**E**) comparison groups

for endometrial receptivity and molecular signaling networks that support embryo implantation and development. Furthermore, through integrated proteomic and transcriptomic analysis, we revealed highly coordinated and stage-specific molecular reprogramming in the goat uterus during the estrous cycle.

WGCNA is a powerful tool for identifying key biological pathways from proteomic data. This approach groups proteins into functional modules based on expression patterns without relying on pre-defined significance thresholds or database completeness. A major advantage of WGCNA is its ability to reveal functional networks independent of existing annotation quality, making it particularly suitable for exploring novel protein interactions and cellular responses to environmental changes [16]. In the luteal-phase uterus of high-fecundity goats, elevated expression of genes such as IDH2, PSAT1, MDH1, UBQLN1, RPLP1, SEC23B, RAD23B, PSPH, and MTHFD2, identified from the WGCNA module associated with high fecundity, may contribute to reproductive efficiency through multiple molecular pathways. IDH2, a key enzyme in the tricarboxylic acid (TCA) cycle, catalyzes the conversion of isocitrate to α-ketoglutarate (α-KG) while reducing NADPH, which supports lipid synthesis and antioxidant responses—critical for maintaining cellular homeostasis and embryonic development [17, 18]. PSAT1, involved in serine synthesis, enhances one-carbon metabolism and nucleotide synthesis, supporting rapid cell proliferation and offering antioxidant protection via glutathione synthesis [19, 20]. MDH1, another TCA cycle enzyme, improves mitochondrial energy metabolism, thereby boosting energy supply for embryonic growth [21, 22]. UBQLN1 contributes to protein quality control and autophagy, ensuring a stable uterine environment [23, 24]. RPLP1 enhances translational capacity, supporting embryonic cell proliferation [25]. SEC23B optimizes protein trafficking and secretion of essential growth factors [26]. RAD23B promotes DNA damage repair, safeguarding embryonic genome integrity [27]. MTHFD2 drives one-carbon metabolism,

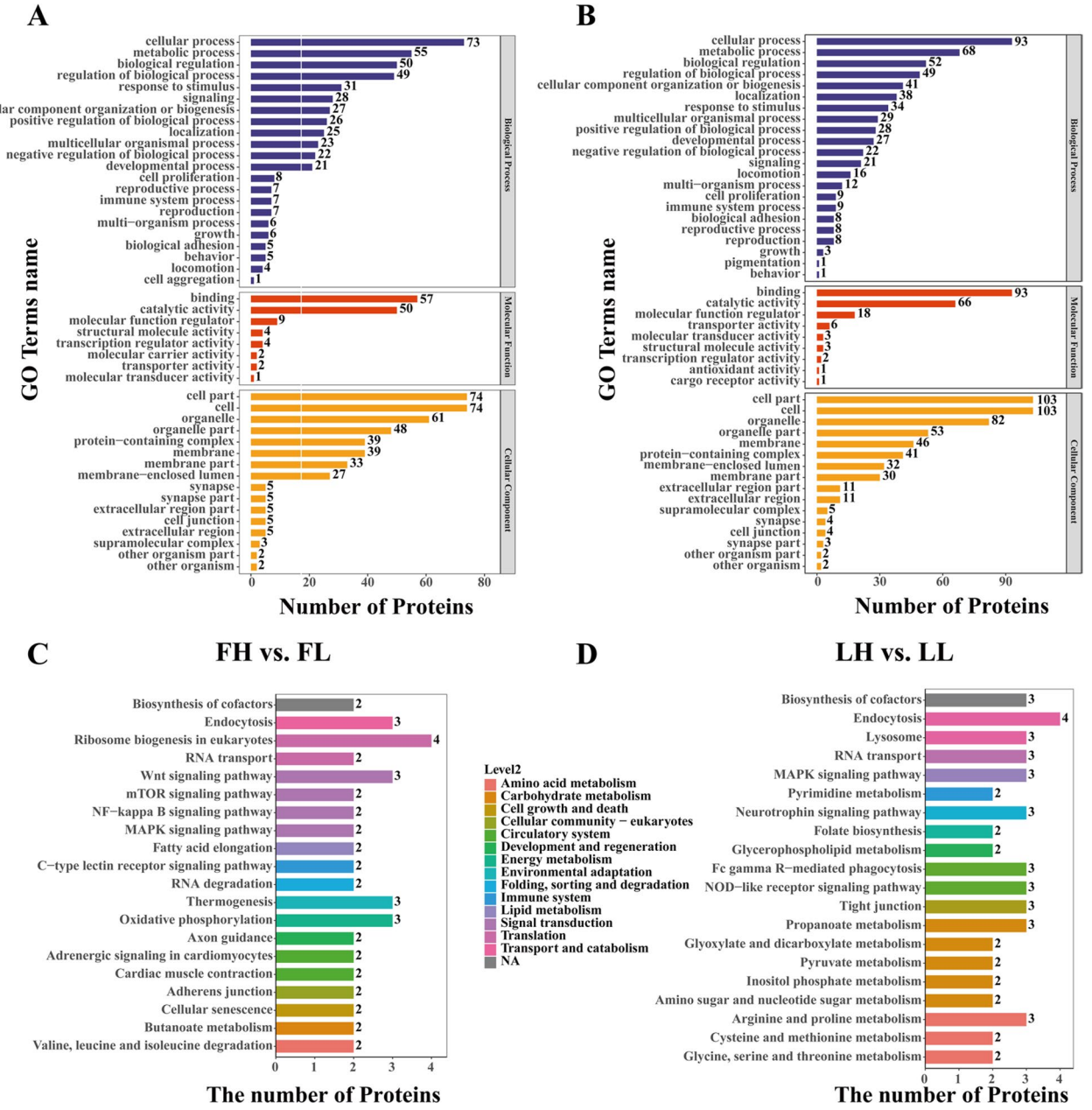

Fig. 5 Gene Ontology (GO) and KEGG pathway enrichment analysis of DAPs in the uterus. **A**, **B** GO functional annotation of DAPs in the FH vs. FL (**A**) and LH vs. LL (**B**) comparison groups. **C**, **D** KEGG pathway classification of DAPs in the FH vs. FL (**C**) and LH vs. LL (**D**) comparison groups

facilitating nucleotide synthesis and supporting rapid embryonic development [28]. Collectively, these genes may enhance energy metabolism, protein synthesis, DNA repair, antioxidant responses, and one-carbon metabolism, thereby creating a favorable intrauterine environment that improves reproductive efficiency.

In this proteomic analysis of uterine tissues from goats, we identified 125 and 183 DAPs during the follicular and luteal phases of the estrous cycle, respectively, representing differential protein abundance between the uterine tissues of high- and low-fecundity goats analyzed separately at each stage. The expression dynamics of these proteins may play important regulatory roles in the high reproductive performance of goats (Capra hircus). Functional annotation and enrichment analysis of the DAPs revealed significant enrichment in two key biological categories: "biological adhesion" and "transporter activity", both of which were markedly upregulated in the uterine tissues of highly prolific goats. Proteins involved in biological adhesion enhance the availability of matrix-derived factors—such as hepatocyte growth factor, fibroblast growth factor 7, insulin-like growth factors (IGF1

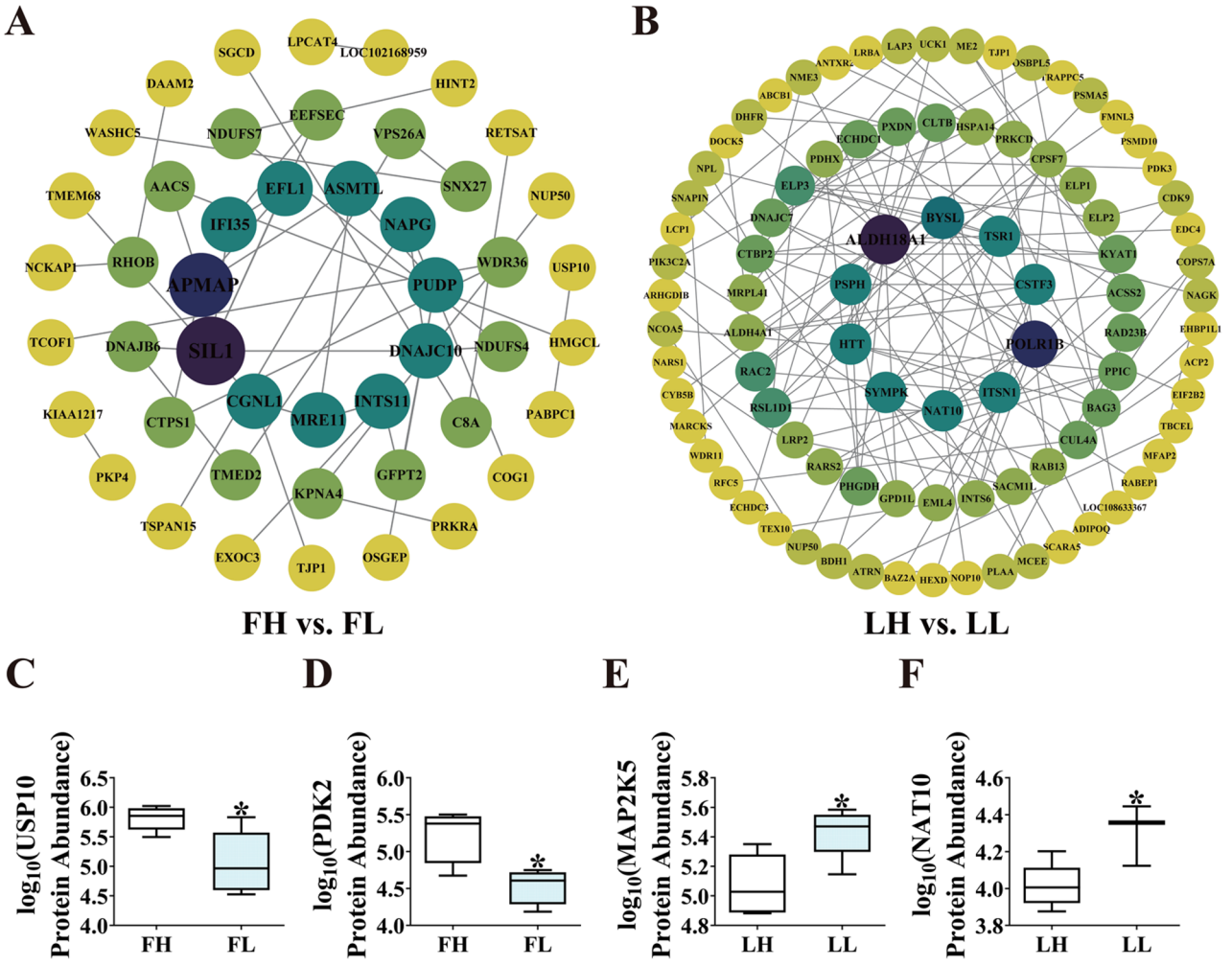

Fig. 6 PPI network of hub DAPs. **A**, **B** PPI analysis of the DAPs was conducted based on the STRING database (https://www.string-db.org/, accessed on 1 August 2025) in FH vs. FL (**A**) and LH vs. LL (**B**) comparison groups; we selected a confidence score of > 0.4 to construct the PPI network; Nodes represent proteins, wiring denote the predicted functional associations. **C-F** Box plots of proteins USP10, PDK2, MAP2K5, and NAT10 are shown. * Presents significant difference at $p < 0.05$

and IGF2)—as well as serum-derived factors including glucose, insulin, and essential amino acids within the uterine lumen [29]. Indeed, many proteins present in the uterine lumen are not directly synthesized by the endometrial epithelium or the conceptus. Establishing and maintaining a uterine luminal microenvironment capable of supporting pregnancy requires epithelial cells to act as selective transporters or barriers. Junctional complexes within epithelial cells help maintain this unique microenvironment by regulating the passage of water, ions, and other small molecules; coordinating the localization of various transporters to sustain appropriate molecular gradients; and modulating cell shape and polarity to facilitate intercellular communication and functionality [30]. In summary, the coordinated upregulation of biological adhesion and transporter activity may represent a key mechanism through which the goat uterus supports high fertility. These processes enhance uterine tissue remodeling, improve nutrient exchange, and optimize the embryonic implantation environment, thereby significantly increasing the likelihood of successful pregnancy establishment and maintenance.

During the follicular phase, the expression levels of PKP4, COL4A1, LPCAT4, and ARRB1 were significantly up-regulated in the high-fertility (FH) group compared to the low-fertility (FL) group. During the follicular phase, these differentially expressed proteins may be associated with sperm selection, early embryonic development, and regulation of the uterine environment. Among these, PKP4 (Plakophilin 4) —a key regulator of intercellular junctions involved in cell adhesion and mechanotransduction—may enhance endometrial mechanical integrity and improve intercellular communication, thereby supporting sperm–uterine interactions and early embryonic development in high-prolificacy goats [31]. COL4A1 (Collagen Type IV Alpha 1 Chain), a major

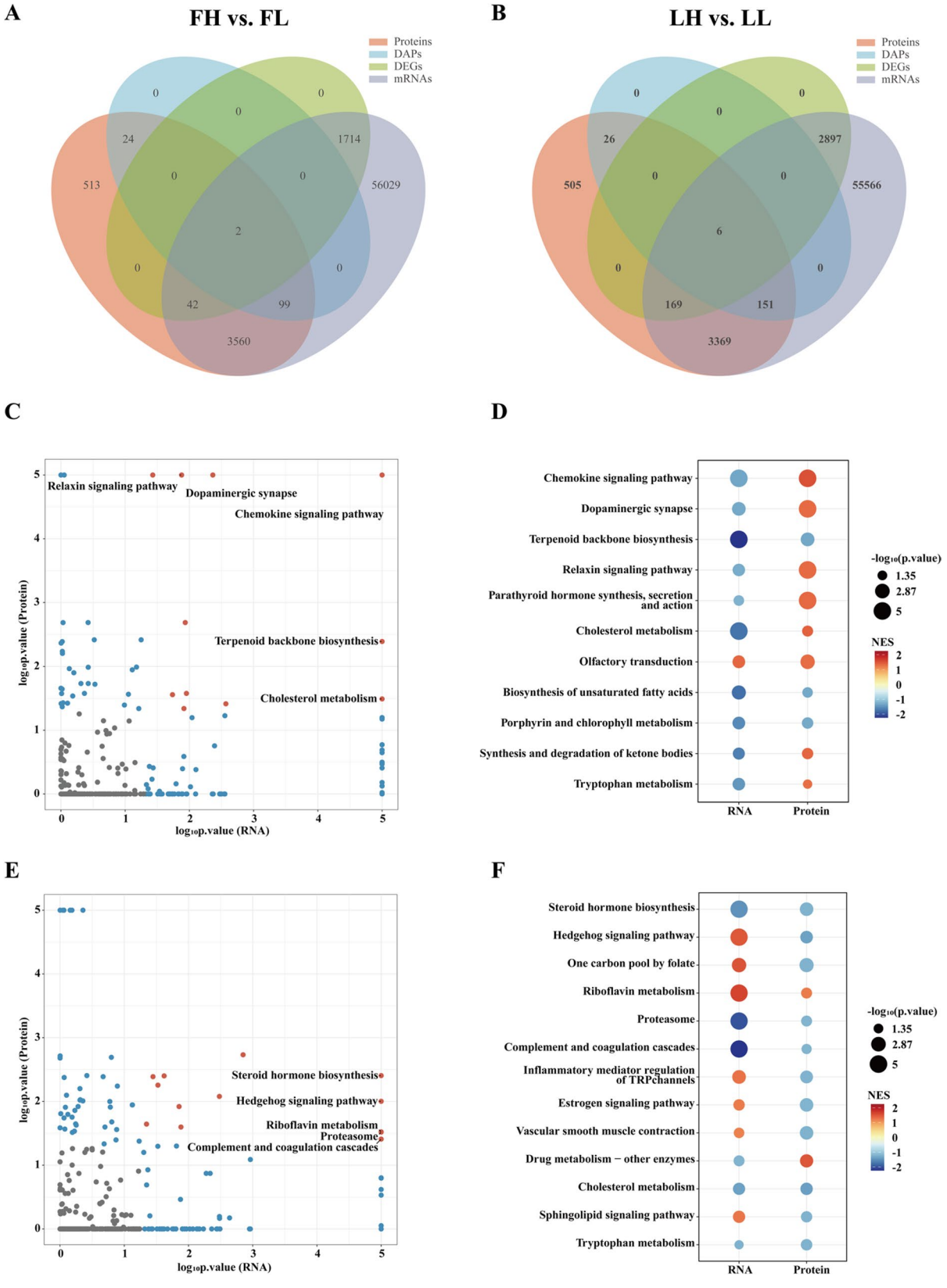

Fig. 7 (See legend on next page.)

(See figure on previous page.)

Fig. 7 Combined analysis of uterine proteomics and transcriptomics. **A**, **B** Venn diagrams showing the overlap between identified proteins and genes in the follicular (**A**) and luteal (**B**) phases. **C**, **E** GSEA pathway enrichment scatter plots for the follicular (**C**) and luteal (**E**) phases. Gray dots represent pathways not significant in either omics dataset; blue indicates pathways significant in only one dataset; red denotes pathways significant in both datasets. **D**, **F** GSEA pathway enrichment bubble plots for the follicular (**D**) and luteal (**F**) phases. Bubble size corresponds to p-value magnitude, and bubble color reflects the distribution of NES values

component of the basement membrane, likely contributes to endometrial structural stability and angiogenesis. Its up-regulation in high-fertility goats may improve basement membrane integrity, promote vascularization, and enhance nutrient supply, thereby supporting early embryonic development and preparing the endometrium for subsequent implantation [32, 33]. LPCAT4 (Lysophosphatidylcholine Acyltransferase 4), which participates in lipid metabolism and membrane synthesis, may optimize the endometrial environment for early embryonic development by modulating lipid composition, membrane fluidity, and signal transduction in high-prolificacy goats [34]. ARRB1 (Arrestin Beta 1), a regulator of G protein-coupled receptors that modulates multiple signaling pathways, may improve hormonal responsiveness and promote cell proliferation in the endometrium, creating a favorable microenvironment for early embryonic development and subsequent implantation [35].

In contrast, several reproduction-related proteins, including MFAP2, SLC30A9, and LRP2, showed a down-regulation trend. MFAP2 (microfibril-associated protein 2) modulates the FAK–AKT signaling pathway, influencing cell proliferation and apoptosis. MFAP2 down-regulation may impair uterine cellular functions and reduce reproductive efficiency [36]. SLC30A9 (zinc transporter 9) is critical for zinc ion transport, which is essential for cellular signaling, gene expression, and immune regulation. Reduced expression may disrupt zinc homeostasis, adversely affecting cell proliferation and differentiation within the uterus, ultimately impairing embryonic development and placental function [37]. LRP2 (low-density lipoprotein receptor-related protein 2) is involved in nutrient uptake, signal transduction, and metabolic regulation. LRP2 down-regulation may disturb uterine lipid metabolism and nutrient transport, compromising the energy supply required for embryonic development [38].

Notably, protein expression in the uterus during the luteal phase differs from that in the follicular phase. Proteins such as HSD11B2 (hydroxysteroid 11-beta dehydrogenase 2) and SMOC2 (secreted modular calcium-binding protein 2) may contribute to the establishment and maintenance of pregnancy by modulating hormonal activity, remodeling the cellular microenvironment, and optimizing energy metabolism, thereby collectively fostering a highly favorable uterine microenvironment. The Hsd11b2 enzyme converts cortisol to its inactive form, cortisone, thereby regulating local glucocorticoid levels [39]. Given that glucocorticoids are known to modulate progesterone, high HSD11B2 expression may consequently influence progesterone levels to help create a uterine environment favorable for embryo survival and development [40]. SMOC2, a recently characterized non-structural component of the extracellular matrix (ECM), is highly upregulated during tissue remodeling [41]. Elevated expression of SMOC2 likely suggests that the uterus of high-prolificacy goats undergoes more active and efficient tissue reconstruction and vascularization. We further focused on proteins related to embryonic development during the luteal phase. Among the down-regulated proteins, SERPINA5, CDK9, and HDAC7 were highlighted. SERPINA5, a serine protease inhibitor, plays important roles in coagulation, inflammation, and fibrinolysis. Its down-regulation in high-prolificacy goats may promote an anticoagulant and anti-inflammatory uterine microenvironment, thereby improving endometrial receptivity and supporting the attachment and development of multiple embryos [42]. CDK9, a key transcriptional kinase, regulates RNA polymerase II-mediated elongation of genes involved in cell cycle progression, differentiation, and stress responses. Reduced CDK9 expression may allow more precise temporal control of gene expression during endometrial remodeling during implantation, optimizing the uterus for multiple embryo implantations [43]. HDAC7, a histone deacetylase, acts as an epigenetic repressor and is involved in vascular development and immune regulation. HDAC7 down-regulation may relieve transcriptional repression of genes critical for embryo implantation, thereby activating programs conducive to high prolificacy [44].

Proteomic analysis is a scientific discipline focused on protein expression, functions, and interactions [45]. As primary executors of cellular functions, proteins are central to understanding the complexity of biological systems and intracellular processes [46, 47]. Proteomics also aids in identifying proteins linked to phenotypic traits, revealing underlying molecular mechanisms and potential biomarkers. Advances in proteomics have driven improvements in mass spectrometry, bioinformatics, and data analysis, providing powerful tools for biological research. Similarly, transcriptomics involves the comprehensive study of all transcripts (mainly mRNAs) in a specific cell or tissue under given conditions [48]. Using high-throughput sequencing technologies, it enables systematic analysis of gene expression levels, splice variants, non-coding RNAs, and other features, playing a crucial

role in understanding gene regulation, cellular states, and functional mechanisms. Transcriptomic data provide a gene-level blueprint for interpreting biological processes and are often integrated with proteomic data to elucidate the multi-level regulation from genes to functional outcomes.

A comparative analysis of uterine proteomic and transcriptomic data across different reproductive stages revealed that the number of detected transcripts far exceeded that of proteins—a common phenomenon reflecting the frequent discordance or lag between transcriptional and translational levels. In the present study, integrated transcriptomic and proteomic analyses of the goat uterus revealed distinct pathway enrichment patterns between the follicular and luteal phases, suggesting phase-specific regulatory mechanisms. During the follicular phase, significant enrichment was observed in the relaxin signaling pathway. In the uterus, relaxin promotes tissue remodeling, extracellular matrix degradation, and angiogenesis, which may facilitate preparatory changes for potential embryo implantation [49, 50]. Concurrent enrichment in the terpenoid backbone biosynthesis pathway may suggests active synthesis of cholesterol and steroid hormone precursors, which could support the high metabolic demands and steroid-mediated signaling within the uterine environment during this stage [51].

It should be noted that the current analysis, integrating proteomic and transcriptomic data, remains at a descriptive bioinformatic level. While we have identified differentially expressed genes and proteins hypothesized to be associated with target traits, these findings should be interpreted with caution. Conclusive evidence regarding their specific biological roles is pending experimental validation. Further functional studies, including Western blot and qPCR, are required to characterize the key candidate genes and verify their functions.

Conclusion

In this study, we conducted an integrated DIA proteomic and transcriptomic analysis of uterine tissues from Yunshang black goats during the follicular and luteal phases of the estrous cycle. We identified key protein co-expression modules and hub proteins—such as IDH2, PSAT1, MDH1, and others—that are potentially closely associated with high fecundity. Functional enrichment analyses revealed that biological adhesion and transporter activity are likely critical processes supporting uterine receptivity and embryonic development. Moreover, stage-specific pathway activations, including the relaxin signaling pathway during the follicular phase and terpenoid backbone biosynthesis during the luteal phase, may underscore the dynamic molecular reprogramming of the uterus. These findings provide novel insights into the proteomic and transcriptomic basis of uterine prolificacy in goats and offer valuable resources for future molecular breeding strategies aimed at enhancing reproductive efficiency in livestock. It should be noted that the current conclusions, derived from bioinformatic analyses, require further validation through functional experiments to definitively establish the roles of the identified candidates.

Abbreviations

DAPs	Differentially Abundant Proteins
DDA	Data-Dependent Acquisition
DEGs	Differentially Expressed Genes
DIA	Data-Independent Acquisition
ECM	Extracellular Matrix
FASP	Filter-Aided Sample Preparation
FC	Fold Change
FDR	False Discovery Rate
FH/FL	High-/Low-Fecundity group in the Follicular phase
LH/LL	High-/Low-Fecundity group in the Luteal phase
GO	Gene Ontology
GSEA	Gene Set Enrichment Analysis
KEGG	Kyoto Encyclopedia of Genes and Genomes
MS	Mass Spectrometry
PCA	Principal Component Analysis
PPI	Protein-Protein Interaction
RNA-Seq	RNA Sequencing
WGCNA	Weighted Gene Co-expression Network Analysis

Supplementary Information

The online version contains supplementary material available at https://doi.org/10.1186/s12864-026-12634-w.

Supplementary Material 1.

Supplementary Material 2.

Acknowledgements

Thanks to all participants for their advice and support of this study.

Authors' contributions

D.B.Z: Formal Analysis, Data Curation, Writing-Original Draft. X.L.D: Formal Analysis, Data Curation. Y.F.L: Data Curation. M.Y.F: Data Curation, Writing-Original Draft. M.X.C: Methodology, Writing Review and Editing.

Funding

This work was financially supported by the National Natural Science Foundation of China (32102509), the Agricultural Science and Technology Innovation Program of China (ASTIP-IAS13) and the Earmarked Fund for China Agriculture Research System of MOF and MARA (CARS-38-02).

Data availability

Proteomics data can be found at http://proteomecentral.proteomexchange.org/cgi/GetDataset?ID=PXD071898. RNA-seq data can be found at https://www.ncbi.nlm.nih.gov/bioproject/PRJNA1379274.

Declarations

Ethics approval and consent to participate

The participates in our study written informed consent. In this research, animal samples were approved by the Institute of Animal Science, Chinese Academy of Agricultural Sciences, Beijing, China. Ethical oversight was given by the Animal Ethics Committee of the IAS-CAAS (No. IAS2019-63).

Consent for publication

Not applicable.

Competing interests

The authors declare no competing interests.

Author details
[1]State Key Laboratory of Animal Biotech Breeding, Institute of Animal Science, Chinese Academy of Agricultural Sciences (CAAS), No. 2 Yuanmingyuan West Rd, Beijing 100193, China
[2]Department of Animal Genetics and Breeding, National Engineering Laboratory for Animal Breeding, MARA Laboratory of Animal Genetics and Breeding, College of Animal Science and Technology, China Agricultural University (CAU), Beijing 100193, China
[3]Henan University (HENU), Zhengzhou 450046, China

Received: 26 November 2025 / Accepted: 4 February 2026
Published online: 21 February 2026

References

1. Li Z, Jiang Y, Khan M, Xue B, Zhao X, Fu B, Li W, Danzeng B, Ni X, Shao Q, Ouyang Y. Dietary energy and protein levels influence the mutton quality and metabolomic profile of the Yunshang black goat. Foods. 2024;13(14):2271.
2. Brosens J. O-092 Does embryo biosensing really determine endometrial fate decisions at implantation? Hum Reprod. 2023;38:(Supplement_1).
3. Sieg W, Kiewisz J, Podolak A, Jakiel G, Woclawek-Potocka I, Lukaszuk J, Lukaszuk K. Inflammation-Related molecules at the Maternal-Fetal interface during pregnancy and in pathologically altered endometrium. Curr Issues Mol Biol. 2022;44(9):3792–808.
4. Xu X, Zhou Y, Fu B, Wei H. Uterine NK cell functions at maternal-fetal interface. Biol Reprod. 2022;107(1):327–38.
5. Huang Q, Ding J, Gong M, Wei M, Zhao Q, Yang J. Effect of miR-30e regulating NK cell activities on immune tolerance of maternal-fetal interface by targeting PRF1. Biomed Pharmacother. 2019;109:1478–87.
6. Krause C, Schaake S, Grütz K, Sievert H, Reyes CJ, König IR, Laabs BH, Jamora RD, Rosales RL, Diesta CCE, Pozojevic J, Gemoll T, Westenberger A, Kaiser FJ, Klein C, Kirchner H. DNA methylation as a potential molecular mechanism in X-linked Dystonia-Parkinsonism. Mov Disord. 2020;35(12):2220–9.
7. Wang S, Shi JT, Wang XR, Mu HX, Wang XT, Xu KY, Wang QS, Chen SW. 1H-Indazoles derivatives targeting PI3K/AKT/mTOR pathway: Synthesis, antitumor effect and molecular mechanism. Bioorg Chem. 2023;133:106412.
8. Yang Q, Liu J, Wang Y, Zhao W, Wang W, Cui J, Yang J, Yue Y, Zhang S, Chu M, Lyu Q, Ma L, Tang Y, Hu Y, Miao K, Zhao H, Tian J, An L. A proteomic atlas of ligand-receptor interactions at the ovine maternal-fetal interface reveals the role of histone lactylation in uterine remodeling. J Biol Chem. 2022;298(1):101456.
9. Demant M, Deutsch DR, Fröhlich T, Wolf E, Arnold GJ. Proteome analysis of early lineage specification in bovine embryos. Proteomics. 2015;15(4):688–701.
10. La Y, Tang J, Guo X, Zhang L, Gan S, Zhang X, Zhang J, Hu W, Chu M. Proteomic analysis of sheep uterus reveals its role in prolificacy. J Proteom. 2020;210:103526.
11. Schwanhäusser B, Busse D, Li N, Dittmar G, Schuchhardt J, Wolf J, Chen W, Selbach M. Global quantification of mammalian gene expression control. Nature. 2011;473(7347):337–42.
12. Langfelder P, Horvath S. WGCNA: an R package for weighted correlation network analysis. BMC Bioinformatics. 2008;9:559.
13. Thakur S, Rohilla J, Kumar K, Kumar H, Singh R, Kaur V, Kamboj R, Kaur R. Synthesis of a trinuclear zinc(II) cluster composed of [4.4.3.0(1,5)]tridecane cages: a rapid detection and degradation probe for the chemical warfare agent simulant diethyl cyanophosphonate in protein-rich food products. Analyst. 2023;148(11):2582–93.
14. Mistry J, Chuguransky S, Williams L, Qureshi M, Salazar GA, Sonnhammer ELL, Tosatto SCE, Paladin L, Raj S, Richardson LJ, Finn RD, Bateman A. Pfam: the protein families database in 2021. Nucleic Acids Res. 2021;49(D1):D412–9.
15. Quevillon E, Silventoinen V, Pillai S, Harte N, Mulder N, Apweiler R, Lopez R. InterProScan: protein domains identifier. Nucleic Acids Res. 2005;33:W116–120.
16. Carr AV, Frey BL, Scalf M, Cesnik AJ, Rolfs Z, Pike KA, Yang B, Keller MP, Jarrard DF, Shortreed MR, Smith LM. MetaNetwork enhances biological insights from quantitative proteomics differences by combining clustering and enrichment analyses. J Proteome Res. 2022;21(2):410–9.
17. Zhang GF, Jensen MV, Gray SM, El K, Wang Y, Lu D, Becker TC, Campbell JE, Newgard CB. Reductive TCA cycle metabolism fuels glutamine- and glucose-stimulated insulin secretion. Cell Metab. 2021;33(4):804–17.
18. Xu W, Yang H, Liu Y, Yang Y, Wang P, Kim SH, Ito S, Yang C, Wang P, Xiao MT, Liu LX, Jiang WQ, Liu J, Zhang JY, Wang B, Frye S, Zhang Y, Xu YH, Lei QY, Guan KL, Zhao SM, Xiong Y. Oncometabolite 2-hydroxyglutarate is a competitive inhibitor of α-ketoglutarate-dependent dioxygenases. Cancer Cell. 2011;19(1):17–30.
19. Zheng P, Hu Z, Shen Y, Gu L, Ouyang Y, Duan Y, Ji G, Dong B, Lin Y, Wen T, Tian Q, Hou Y, Zhou Q, Sun X, Chen X, Wang KL, Luo S, Wu S, Sun Y, Li M, Xiao L, Wu Q, Meng Y, Liu G, Wang Z, Bai X, Duan S, Ding Y, Bi Y, Wang Y, Li G, Liu X, Lu Z, Wu X, Tang Z, Xu D. PSAT1 impairs ferroptosis and reduces immunotherapy efficacy via GPX4 hydroxylation. Nat Chem Biol. 2025;21(9):1420–32.
20. Yang M, Vousden KH. Serine and one-carbon metabolism in cancer. Nat Rev Cancer. 2016;16(10):650–62.
21. Kang S, Antoniewicz MR, Hay N. Metabolic and transcriptomic reprogramming during contact inhibition-induced quiescence is mediated by YAP-dependent and YAP-independent mechanisms. Nat Commun. 2024;15(1):6777.
22. Qiao L, Zhuang Z, Wang Y, Xie K, Zhang X, Shen Y, Song J, Zhou S. Nocturnin promotes NADH and ATP production for juvenile hormone biosynthesis in adult insects. Pest Manag Sci. 2025;81(6):3103–11.
23. Yu Y, Pang D, Huang J, Li C, Cui Y, Shang H. Downregulation of Lnc-ABCA12-3 modulates UBQLN1 expression and protein homeostasis pathways in amyotrophic lateral sclerosis. Sci Rep. 2024;14(1):21383.
24. Li Y, Xu J, Chen W, Wang X, Zhao Z, Li Y, Zhang L, Jiao J, Yang Q, Ding Q, Yang P, Wei L, Chen Y, Chen Y, Ruan XZ, Zhao L. Hepatocyte CD36 modulates UBQLN1-mediated proteasomal degradation of autophagic SNARE proteins contributing to septic liver injury. Autophagy. 2023;19(9):2504–19.
25. Yang W, Wang H, Li Z, Zhang L, Liu J, Kirchhoff F, Huan C, Zhang W. RPLP1 restricts HIV-1 transcription by disrupting C/EBPβ binding to the LTR. Nat Commun. 2024;15(1):5290.
26. Yehia L, Liu D, Fu S, Iyer P, Eng C. Non-canonical role of wild-type SEC23B in the cellular stress response pathway. Cell Death Dis. 2021;12(4):304.
27. Cheon NY, Kim HS, Yeo JE, Schärer OD, Lee JY. Single-molecule visualization reveals the damage search mechanism for the human NER protein XPC-RAD23B. Nucleic Acids Res. 2019;47(16):8337–47.
28. Ramos L, Henriksson M, Helleday T, Green AC. Targeting MTHFD2 to exploit Cancer-Specific metabolism and the DNA damage response. Cancer Res. 2024;84(1):9–16.
29. Satterfield MC, Dunlap KA, Hayashi K, Burghardt RC, Spencer TE, Bazer FW. Tight and adherens junctions in the ovine uterus: differential regulation by pregnancy and progesterone. Endocrinology. 2007;148(8):3922–31.
30. Lee RS, Wheeler TT, Peterson AJ. Large-format, two-dimensional polyacrylamide gel electrophoresis of ovine periimplantation uterine luminal fluid proteins: identification of aldose reductase, cytoplasmic actin, and transferrin as conceptus-synthesized proteins. Biol Reprod. 1998;59(4):743–52.
31. Müller L, Hatzfeld M. Emerging functions of plakophilin 4 in the control of cell contact dynamics. Cell Commun Signal. 2025;23(1):109.
32. Tambala D, Vassar R, Snow J, Balestrini S, Bersano A, Guey S, Bonaventura E, Signorini S, Sartori S, Bertini E, Tonduti D, Parazzini C, Macchiaiolo M, Pelizza MF, Pichiecchio A, Massella L, Coste T, Orcesi S, Politano D, Bacci G, Marziali E, Dollfus H, Mandelli A, Chinali M, Plaisier E, Simioni P, Colombatti R, Guerrini R, Tournier-Lasserve E, Gould DB, Musolino PL. COL4A1 and COL4A2-related disorders: clinical features, diagnostic guidelines, and management. Genet Med. 2025;27(9):101514.
33. Guo J, Ma X, Liu D, Wang F, Xia J, Zhang B, Zhao P, Zhong F, Chen L, Long Q, Jiang L, Zhang S, Liao N, Wang J, Wu W, Sun J, Huang M, Cheng Z, Huang G, Zou C. A distinct subset of urothelial cells with enhanced EMT features promotes chemotherapy resistance and cancer recurrence by increasing COL4A1-ITGB1 mediated angiogenesis. Drug Resist Updat. 2024;76:101116.
34. Mason AS, Varley CL, Foody OM, Li X, Skinner K, Walker D, Larson TR, Wakamatsu D, Baker SC, Southgate J. LPCAT4 knockdown alters barrier integrity and cellular bioenergetics in human urothelium. Int J Mol Sci. 2022;23(19):11871.
35. Ye Y, Jiang H, Wu Y, Wang G, Huang Y, Sun W, Zhang M. Role of ARRB1 in prognosis and immunotherapy: A Pan-Cancer analysis. Front Mol Biosci. 2022;9:1001225.
36. Deng Y, Huang X, Yang Y, Zhang Y, Zeng B, Bao Y, Cao L, Wang X, Ma L, Wang J. MFAP2 upregulation promotes ESCC metastasis via FAK-AKT signaling pathway. Faseb J. 2024;38(24):e70266.
37. Deng H, Qiao X, Xie T, Fu W, Li H, Zhao Y, Guo M, Feng Y, Chen L, Zhao Y, Miao L, Chen C, Shen K, Wang X. SLC-30A9 is required for Zn(2+) homeostasis, Zn(2+) mobilization, and mitochondrial health. Proc Natl Acad Sci U S A. 2021;118(35):e2023909118.

38. Kur E, Mecklenburg N, Cabrera RM, Willnow TE, Hammes A. LRP2 mediates folate uptake in the developing neural tube. J Cell Sci. 2014;127(Pt 10):2261–8.
39. Theodoridi A, Dinarello A, Badenetti L, Pavlidis M, Dalla Valle L, Tsalafouta A. Knockout of the hsd11b2 gene extends the cortisol stress response in both zebrafish larvae and adults. Int J Mol Sci. 2021;22(22):12525.
40. Solano ME, Arck PC. Steroids, pregnancy and fetal development. Front Immunol. 2019;10:3017.
41. Feng D, Gao P, Henley N, Dubuissez M, Chen N, Laurin LP, Royal V, Pichette V, Gerarduzzi C. SMOC2 promotes an epithelial-mesenchymal transition and a pro-metastatic phenotype in epithelial cells of renal cell carcinoma origin. Cell Death Dis. 2022;13(7):639.
42. Hayashi KG, Ushizawa K, Hosoe M, Takahashi T. Differential gene expression of Serine protease inhibitors in bovine ovarian follicle: possible involvement in follicular growth and Atresia. Reprod Biol Endocrinol. 2011;9:72.
43. Tellier M, Zaborowska J, Neve J, Nojima T, Hester S, Fournier M, Furger A, Murphy S. CDK9 and PP2A regulate RNA polymerase II transcription termination and coupled RNA maturation. EMBO Rep. 2022;23(10):e54520.
44. Wang Y, Abrol R, Mak JYW, Das Gupta K, Ramnath D, Karunakaran D, Fairlie DP, Sweet MJ. Histone deacetylase 7: a signalling hub controlling development, inflammation, metabolism and disease. Febs J. 2023;290(11):2805–32.
45. Ding Z, Wang N, Ji N, Chen ZS. Proteomics technologies for cancer liquid biopsies. Mol Cancer. 2022;21(1):53.
46. Zhou B, Jiang ZH, Dai MR, Ai YL, Xiao L, Zhong CQ, Wu LZ, Chen QT, Chen HZ, Wu Q. Full-length GSDME mediates pyroptosis independent from cleavage. Nat Cell Biol. 2024;26(9):1545–57.
47. Geng L, Gao W, Saiyin H, Li Y, Zeng Y, Zhang Z, Li X, Liu Z, Gao Q, An P, Jiang N, Yu X, Chen X, Li S, Chen L, Lu B, Li A, Chen G, Shen Y, Zhang H, Tian M, Zhang Z, Li J. MLKL deficiency alleviates neuroinflammation and motor deficits in the α-synuclein Transgenic mouse model of parkinson's disease. Mol Neurodegener. 2023;18(1):94.
48. Huang Y, Zhu S, Yao S, Zhai H, Liu C, Han JJ. Unraveling aging from transcriptomics. Trends Genet. 2025;41(3):218–35.
49. Huang SC, Liu KL, Chen P, Xu BW, Ding WL, Yue TJ, Lu YN, Li SY, Li JK, Jian FC. New insights into the combined effects of aflatoxin B1 and Eimeria ovinoidalis on uterine function by disrupting the gut-blood-reproductive axis in sheep. Microbiome. 2024;12(1):269.
50. MacLennan AH. Relaxin–a review. Aust N Z J Obstet Gynaecol. 1981;21(4):195–202.
51. Lake J, Bortolasci CC, Stuart AL, Pasco JA, Kidnapillai S, Spolding B, Truong TTT, Panizzutti B, Liu ZSJ, Dean OM, Crowley T, Richardson M, Kim JH, Berk M, Williams LJ, Walder K. Metformin is protective against the development of mood disorders. Pharmacopsychiatry. 2023;56(1):25–31.

Publisher's note